The Astrophysical Journal, 996:57 (8pp), 2026 January 1 https://doi.org/10.3847/1538-4357/ae22d4

Collapse of Rotating Very Massive Stellar Cores Leading to a Black Hole and a Massive Disk as a Source of Gravitational Waves

Masaru Shibata[1,2] and Sho Fujibayashi[1,3,4]
[1] Max-Planck-Institut für Gravitationsphysik (Albert-Einstein-Institut), Am Mühlenberg 1, D-14476 Potsdam-Golm, Germany
[2] Center for Gravitational Physics and Quantum Information, Yukawa Institute for Theoretical Physics, Kyoto University, Kyoto, 606-8502, Japan
[3] Frontier Research Institute for Interdisciplinary Sciences, Tohoku University, Aramaki aza Aoba 6-3, Aoba-ku, Sendai 980-8578, Japan
[4] Astronomical Institute, Graduate School of Science, Tohoku University, Sendai 980-8578, Japan
Received 2025 September 16; revised 2025 November 5; accepted 2025 November 19; published 2025 December 24

Abstract

We derive models of rotating very massive stellar cores with mass $\approx 10^2$–$10^4\ M_\odot$ that are marginally stable to the pair-unstable collapse, assuming that the core is isentropic and composed primarily of oxygen. It is shown that cores with mass $\lesssim 10^3\ M_\odot$ can form a massive disk with the mass more than 10% of the core mass around the formed black hole if the core is rotating with more than 30% of the Keplerian limit. We also indicate that the formation of rapidly spinning massive black holes such as the black holes of GW231123 naturally accompanies massive disk formation. By using the result of our previous study, which showed that the massive disk is unstable to the nonaxisymmetric deformation, we predict the amplitude and frequency of gravitational waves and show that the collapse of rotating very massive stellar cores can be a promising source of gravitational waves for the Einstein Telescope. The detection of such gravitational waves will provide us with important information about the formation process of intermediate mass black holes.

Unified Astronomy Thesaurus concepts: Gravitational wave sources (677)

1. Introduction

Metal-poor very massive stars with initial mass larger than $\sim 260\ M_\odot$ are believed to collapse into a black hole after the onset of the electron–positron pair creation instability (referred to as pair instability in the following: C. L. Fryer et al. 2001; A. Heger & S. E. Woosley 2002). Such stars evolve through hydrogen and helium burning, forming a core composed primarily of oxygen (J. R. Bond et al. 1984; D. Arnett 1996), and eventually become unstable to the pair instability, collapsing into a black hole. Such very massive stars are a plausible origin for intermediate-mass black holes.

In the presence of a certain amount of angular momentum, the fate of the collapse could be rich because a disk should be formed around the formed black hole (H. Uchida et al. 2019). In the presence of a massive disk, the remnant can be a source of energetic phenomena such as a gamma-ray burst and an energetic supernova (e.g., C. L. Fryer et al. 2001; A. Heger & S. E. Woosley 2002; H. Uchida et al. 2019; D. M. Siegel et al. 2022; O. Gottlieb et al. 2025). Such a system can be also a strong gravitational-wave emitter if the remnant disk is massive enough, i.e., the disk mass is larger than $\sim$10% of the black hole mass (K. Kiuchi et al. 2011; O. Korobkin et al. 2011; M. Shibata et al. 2021). In this paper, we will point out that the collapse of very massive stellar cores with mass $\lesssim 10^3\ M_\odot$ can form a massive disk around the formed black hole if the surface of the core rotates with the angular velocity that is $\gtrsim$30% of the Keplerian one, and as a result, the remnant can be a strong emitter of gravitational waves, in particular, for the Einstein Telescope (S. Hild et al. 2011) if the mass of the formed black holes is $\lesssim 200\ M_\odot$.

In a recent paper (A. G. Abac et al. 2025), the discovery of a high-mass binary black hole (GW231123) was reported. In this event, masses of two black holes are estimated to be $137^{+22}_{-17} M_\odot$ and $103^{+20}_{-52} M_\odot$ with 90% credible intervals, and dimensionless spins for each black hole are quite high, $0.90^{+0.10}_{-0.19}$ and $0.80^{+0.20}_{-0.51}$, respectively. If the black holes of GW231123 were formed from a collapse of a massive, rapidly rotating stellar core with mass $>140\ M_\odot$, it was likely to be evolved from a rotating very massive star with initial mass larger than $260\ M_\odot$ (see, e.g., K. Takahashi et al. 2018; D. Croon et al. 2025; F. Kıroğlu et al. 2025; S. A. Popa & S. E. de Mink 2025; J. Stegmann et al. 2025; A. Tanikawa et al. 2025 for formation scenarios). H. Uchida et al. (2019) already provided a numerical model for the formation of such a heavy black hole using a progenitor model based on a stellar evolution calculation for a rapidly rotating metal-poor star by K. Takahashi et al. (2018) and a numerical-relativity simulation with relevant physical input (see also O. Gottlieb et al. 2025 for a more simplified model). However, in our previous work, we studied only one particular model for heavy black hole formation. One motivation of our series of works will be to systematically clarify the formation process of heavy black holes for a wide range of core masses $M \approx 10^2$–$10^4\ M_\odot$, for which the collapse is triggered by the pair instability (Y. B. Zeldovich & I. D. Novikov 1971; M. Shibata et al. 2025; for even heavier stars (supermassive stars), the collapse is likely to be triggered by the general relativistic instability, S. Chandrasekhar 1964). At the same time, the formation of black hole–massive disk systems can be a source of burst-type gravitational waves because the massive disk can be unstable against nonaxisymmetric deformation. The primary purpose of this paper is to point out this possibility based on numerical results of M. Shibata et al. (2021); if the black holes of GW231123 were formed from the collapse of a rotating very massive stellar core, the collapse itself emitted gravitational waves of a high amplitude. This implies that the formation process of such heavy black holes can be a target of future

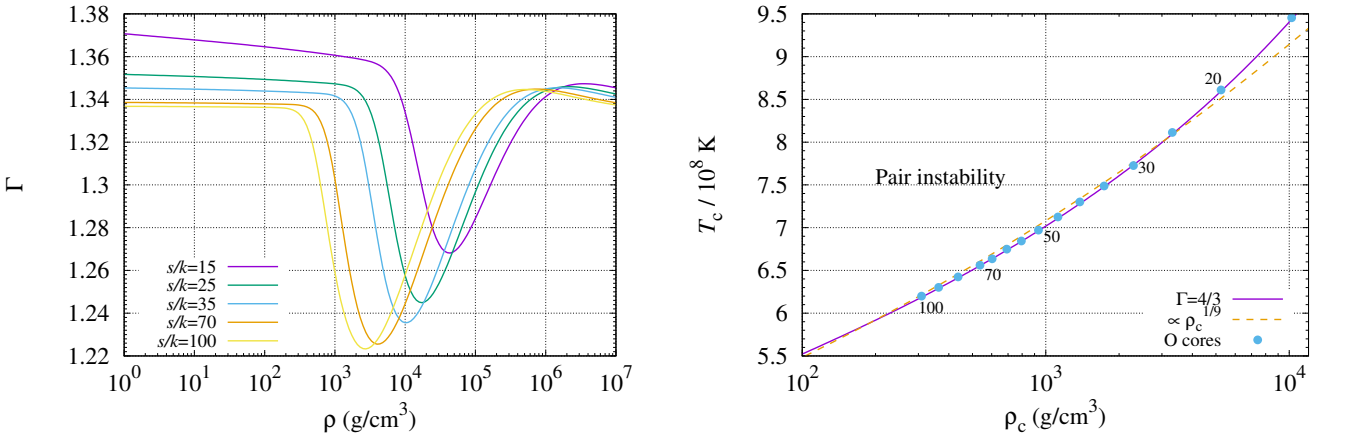

Figure 1. Left: the adiabatic index Γ as a function of the density ρ for $s/k = 15$, 25, 35, 70, and 100. Right: the solid curve denotes the curve of $\Gamma = 4/3$ in the density–temperature plane. The dashed curve denotes a relation of $T \propto \rho^{1/9}$ as an approximation of the solid curve. The filled circles represent the physical information at the center of marginally stable very massive stellar cores with $s/k = 15$, 20, 25, 30, 35, 40, 45, 50, 55, 60, 65, 70, 80, 90, and 100.

ground-based gravitational-wave detectors such as the Einstein Telescope (S. Hild et al. 2011).

This paper is organized as follows: In Section 2, we briefly describe our setup for computing rotating very massive stellar cores in equilibrium. In Section 3, the properties of such stellar cores are summarized, with particular attention paid to the rotational effect. In Section 4, we predict the remnant of the collapse of rotating very massive stellar cores and show that the remnant can be a rapidly spinning black hole surrounded by a massive disk if the core is moderately rapidly rotating. In Section 5, the predicted properties of gravitational waves emitted from unstable massive disks orbiting black holes with mass in the range of 50–200 $M_\odot$ are summarized, indicating that the gravitational waves can be a source for the Einstein Telescope (S. Hild et al. 2011). Section 6 is devoted to a summary. Throughout this paper, c, G, and k denote the speed of light, gravitational constant, and Boltzmann's constant, respectively.

2. Setup

We numerically compute equilibrium states of rotating very massive stellar cores in general relativity that are marginally stable to pair instability (Y. B. Zeldovich & I. D. Novikov 1971) as the plausible initial condition for the pair-unstable collapse. According to stellar evolution calculations (e.g., K. Takahashi et al. 2016, 2018), very massive stars become pair unstable at a late phase of the evolution at which oxygen–carbon cores become sufficiently massive. In such a stage, the oxygen–carbon core is nearly isentropic, and the mass fraction of oxygen is much larger than that of carbon. Thus, we employ a Timmes–Swesty equation of state (F. X. Timmes & F. D. Swesty 2000) with the assumption that the stellar core is composed of fully ionized oxygens, electrons, positrons, and photons assuming uniform entropy per baryon, $s = \text{const}$. Specifically, s/k is chosen to be larger than 13, because for smaller values of s/k, very massive star cores are likely to explode after the onset of pair instability (e.g., D. Arnett 1996; C. L. Fryer et al. 2001; K. Takahashi et al. 2016). Note that K. Takahashi et al. (2016) reported the black hole formation from oxygen–carbon cores only with mass larger than $\approx 120\ M_\odot$. Thus, for $s/k \lesssim 14$ for which the oxygen core mass is $\lesssim 128\ M_\odot$ (see Section 3), the oxygen core may explode after the onset of the collapse due to pair instability.

Rigid rotation is assumed following the stellar evolution results for rapidly rotating very massive stars by K. Takahashi et al. (2016, 2018), which showed that the oxygen–carbon cores are broadly rigidly rotating with a weak degree of differential rotation. For example, K. Takahashi et al. (2018) presented the end result for the evolution of a rapidly rotating very massive star with an initial mass 320 $M_\odot$. They found that at the critical density and temperature of the pair-unstable collapse, the core is approximately composed of oxygen and carbon with a mass ratio 9:1 and mass $\approx 150\ M_\odot$ and is surrounded by an extended envelope composed of helium and hydrogen with mass $\sim 140\ M_\odot$. The value of the entropy per baryon for the core is $\approx 15\ k$. H. Uchida et al. (2019) performed an axisymmetric simulation in general relativity for the collapse of this stellar core and indeed showed that the remnant is a rapidly spinning black hole with the mass $\sim 130\ M_\odot$ and the dimensionless spin of ~ 0.8, which is surrounded by a massive compact disk of mass $\sim 20\ M_\odot$.

Our aim is to numerically derive equilibrium stellar cores marginally stable against pair instability. Thus, central values of the density and temperature are determined from the condition of $\Gamma = 4/3$ for a given equation of state with $s = \text{const}$. For the chosen equations of state, the Γ value steeply decreases far below $4/3$ with the increase of the density at such ranges of the density and temperature (see the left panel of Figure 1). On the other hand, for another range of the equation of state with lower density and temperature, the condition of $\Gamma > 4/3$ is always satisfied (see Figure 1). The criterion for the stability depends on compactness and rotational effect of the system (J.-L. Tassoul 1978; S. L. Shapiro & S. A. Teukolsky 1983; M. Shibata et al. 2016). However, these effects change the stability criterion of Γ only by $O(10^{-3})$ in the problem of stars not rotating rapidly, and hence, we simply use $\Gamma = 4/3$ as the critical curve for the stability. Note, however, that for rapidly rotating stellar cores near the mass-shedding limit, the stabilization effect by the rotation can change the critical value of Γ by 5×10^{-3} (M. Shibata et al. 2016), and hence, the instability could happen for a more compact state than that for $\Gamma = 4/3$. It should be also noted that the stellar collapse may have started after the Γ value for a fraction of the matter in the central region becomes smaller than $4/3$; that is, the collapse may have started at slightly more compact state than that we considered in this paper.

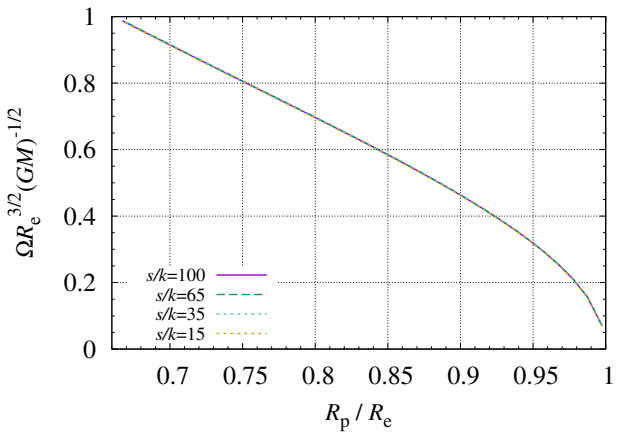

Figure 2. The angular velocity Ω in units of $(GM/R_e^3)^{1/2}$ as a function of R_p/R_e for $s/k = 15$, 35, 65, and 100. The four curves approximately overlap each other.

The left panel of Figure 1 shows Γ as a function of the density for several values of s/k in the range between 15 and 100. Irrespective of the s/k values, Γ is slightly larger than $4/3$ for low-density regions of $\rho \lesssim 10^{2.5}\,\mathrm{g\,cm^{-3}}$ for which the radiation pressure is the major pressure source. For the region of $\rho \approx 10^{2.5}$–$10^{5.5}\,\mathrm{g\,cm^{-3}}$, the value of Γ falls below $4/3$ because of the high temperature sufficient to create electron–positron pairs. For computing equilibrium states of very massive stellar cores, we choose the central density of $\rho_c \approx 10^{2.5}$–$10^{4}\,\mathrm{g\,cm^{-3}}$ for which the Γ value becomes $\approx 4/3$. It is worth noting that the temperature of $\Gamma = 4/3$ is in a narrow range as 6.2–9.5×10^8 K for $\rho \approx 10^{2.5}$–$10^{4}\,\mathrm{g\,cm^{-3}}$ (see the right panel of Figure 1).

The solid curve in the right panel of Figure 1 shows the relation between the density and temperature for $\Gamma = 4/3$. At each point along the curve, the values of s/k are different. For the larger density, the s/k value is smaller: The filled circles show the points of the representative values of $s/k = 15$, 20, 25, 30, 35, 40, 45, 50, 55, 60, 65, 70, 80, 90, and 100. The dashed curve denotes a power-law fitting formula of the solid curve. We find that it is well represented by $T \propto \rho^{1/9}$ or $\rho \propto T^9$ for the range of s/k in which we are interested.

Each model of the rotating stellar cores is determined by giving the axial ratio R_p/R_e, where R_p and R_e denote the polar and equatorial axial lengths, respectively. The numerical method is essentially the same as in our previous papers (e.g., M. Shibata et al. 2025). We confirmed that for $R_p/R_e \lesssim 1$, our model with $s/k = 15$ has a similar structure to that of the oxygen core for a 320 $M_\odot$ model of K. Takahashi et al. (2018). Because the stellar cores considered in this paper are not very compact (compactness defined by $GM/(c^2 R_e)$ is smaller than $\sim 10^{-3}$), the coordinate axial lengths are in agreement with the proper length within $\sim 0.1\%$ error. Figure 2 shows the relation between the angular velocity Ω in units of the Keplerian one $\Omega_{\rm Kep} = (GM/R_e^3)^{1/2}$ as a function of the axial ratio R_p/R_e for $s/k = 15$, 35, 65, and 100. We find that the relation depends only weakly on s/k (i.e., mass M). This is because the equation of state is approximately written as the $\Gamma = 4/3$ polytrope for very massive stars irrespective of the s/k values. In the following, we pay attention to the cases with $R_p/R_e = 2/3$, 0.85, 0.90, and 0.95, for which $\Omega/\Omega_{\rm Kep}$ is $\approx$0.99, 0.59, 0.46, and 0.32, respectively.

3. Properties of Rotating Very Massive Stellar Cores

Before going ahead, we briefly discuss general properties for the cores of very massive stars, which are marginally stable against pair instability. As summarized, e.g., in J. R. Bond et al. (1984) and M. Shibata et al. (2025), the mass of very massive stellar core M is approximately proportional to $(s/k)^2$ for a given chemical composition because their adiabatic indices are close to $4/3$. As shown in the left panel of Figure 3, this is indeed approximately satisfied. Also, the photon radiation always governs the equation of state, and hence, the entropy per baryon is approximately proportional to T_c^3/ρ_c, where ρ_c and T_c denote the central density and central temperature, respectively. Because $\rho_c \propto T_c^9$ is approximately satisfied at the onset of pair instability, we get approximately get $\rho_c \propto s^{-3/2}$ and $T_c \propto s^{-1/6}$.

For such stellar cores, the stellar radius R in units of the gravitational radius GM/c^2 is written approximately as

$$\frac{c^2 R}{GM} \propto \rho_c^{-1/3} M^{-2/3} \propto s^{1/2} M^{-2/3} \propto s^{-5/6} \propto M^{-5/12}, \quad (1)$$

where we used $\rho_c R^3 \propto M$ and considered spherical cores for simplicity. Therefore, the cores of very massive stars marginally stable against pair instability are less compact for the smaller core mass (i.e., smaller values of s/k). As shown in the right panel of Figure 3 and the left panel of Figure 4, these proportionalities are indeed approximately satisfied.

Assuming the rigid rotation of the core, the maximum angular velocity Ω is determined by the mass-shedding limit, i.e.,

$$\Omega \leqslant \Omega_{\rm Kep} = \sqrt{\frac{GM}{R_e^3}}. \quad (2)$$

Since the angular momentum is approximately proportional to $MR_e^2\Omega$, the maximum value of the dimensionless angular momentum defined by $\chi = cJ/(GM^2)$ is approximately proportional to $(R_e/M)^{1/2}$. This implies that the value of χ can be larger for smaller masses, as shown in the right panel of Figure 4. This suggests that for smaller-mass cores, more rapidly spinning black holes can be formed with heavier disks surrounding the black hole. In the next section, we will show that this is indeed the case.

4. Predicted Outcome of the Collapse

Using the same procedure as in M. Shibata & S. L. Shapiro (2002), M. Shibata (2004), and M. Shibata et al. (2016), we predict the outcome of the collapse of rotating very massive stellar cores assuming that during the collapse leading to the formation of a black hole and a disk, the angular momentum transport plays a negligible role. As we already showed in previous work (H. Uchida et al. 2019), the formation of the black hole and disk is achieved in the dynamical timescale of the system; for the core collapse of very massive stars, the core does not experience an appreciable bounce until the formation of the black hole (no formation of a protoneutron star).[5] Therefore, it is reasonable to assume the negligible angular

[5] Note, however, that in the presence of very rapid rotation of the precollapse star, centrifugal bounce may occur.

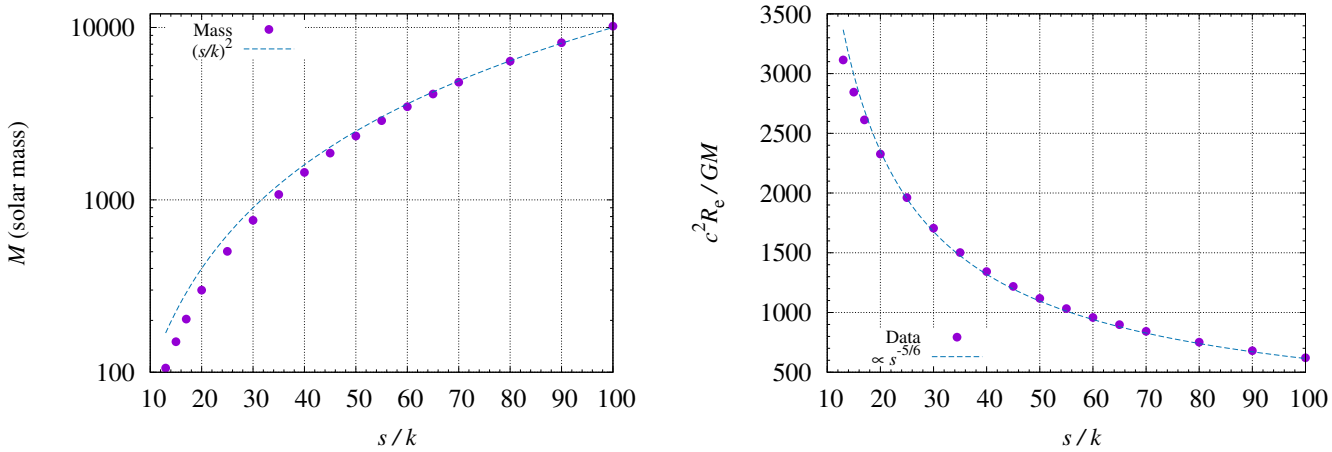

Figure 3. M (left) and $c^2R_e/(GM)$ (right) of very massive stellar cores as functions of s/k with axial ratio, $R_p/R_e = 0.9975$. The dashed curves are $(s/k)^2$ (left) and $\propto s^{-5/6}$ (right).

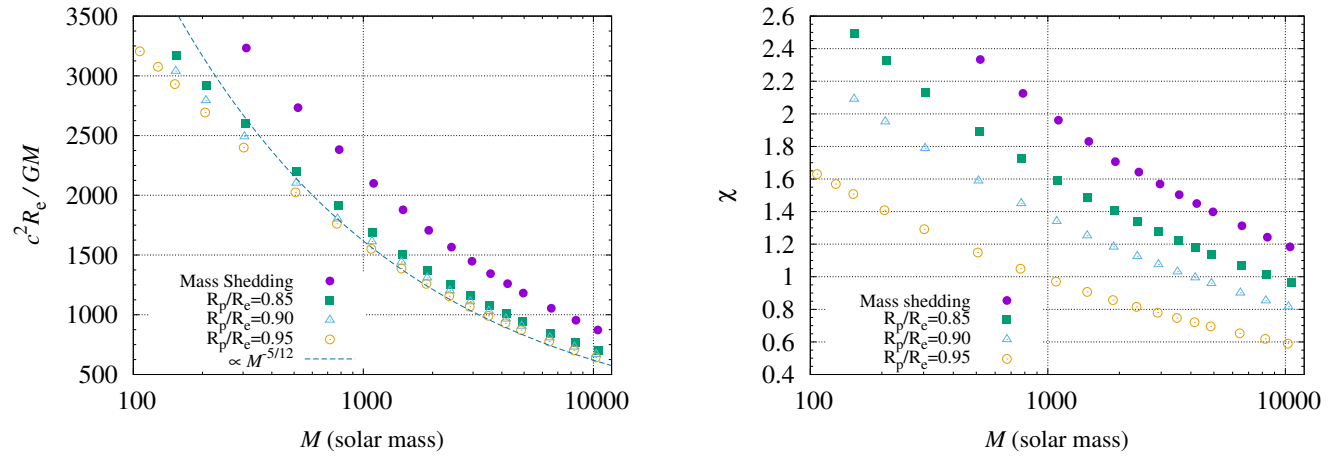

Figure 4. The equatorial radius in units of GM/c^2 (left) and the dimensionless angular momentum $\chi = cJ/(GM^2)$ (right) with constant values of $R_p/R_e = 2/3$, 0.85, 0.90, and 0.95 as functions of the mass. The dashed curve in the left panel denotes $\propto M^{-5/12}$. For $R_pR_e = 2/3$, the stellar cores are close to the mass-shedding limit for which the angular velocity at the equatorial surface is $\approx 0.99\sqrt{GM/R_e^3}$.

momentum transport until the formation of the black hole–disk system. We expect that the angular momentum transport resulting from the magnetohydrodynamics effect will play an important role after the formation of the disk, but the relevant timescale is likely to be longer than the dynamical timescale with which the black hole–disk systems are formed unless the viscosity or magnetic-field strength is extremely high (see, e.g., S. Fujibayashi et al. 2024; M. Shibata et al. 2024).

Under the assumption that the angular momentum transport is negligible, the specific angular momentum, $j = hu_\varphi$, for each fluid element is conserved during the evolution of the system. Here, h and u_φ denote the specific enthalpy and azimuthal component of the 4-velocity with the lower subscript. We then calculate the mass and angular momentum of fluid elements in the oxygen cores with the specific angular momentum lower than the value j, denoted by $m(j)$ and $J(j)$, which satisfy $dm(j)/dj > 0$ and $dJ(j)/dj > 0$ for rigidly rotating objects. Numerical integration for $m(j)$ and $J(j)$ is performed for discrete values of j, and hence, a small numerical error appears in the predicted black hole mass and spin although this does not change our conclusion. Here, the specific angular momentum increases with the increase of the cylindrical radius for $\Omega = \text{const.}$, and thus, we assume that fluid elements with smaller values of j collapse into the inner region earlier; $m(j)$ and $J(j)$ increase, reflecting the distribution of j. Then, it is natural to assume that the mass and angular momentum of a formed black hole increase with time, reflecting the distribution of j.

Assuming that $m(j)$ and $J(j)$ are instantaneous values of the mass and angular momentum of a growing black hole, we can then derive the specific angular momentum of the innermost stable circular orbits of the given black hole (J. M. Bardeen et al. 1972), $j_{\rm ISCO}(j)$, which is also a function of j. Note that the matter outside the black hole is assumed to have a specific angular momentum larger than j. Then, if $j_{\rm ISCO}$ is larger than j, we may consider that further accretion onto the black hole continues. On the other hand, if the condition of $j_{\rm ISCO} \leqslant j$ is satisfied, further accretion is prohibited, and the matter should remain outside the black hole with the mass and angular momentum $m(j_{\rm f})$ and $J(j_{\rm f})$, where $j_{\rm f}$ denotes the value of j, which satisfies $j_{\rm ISCO}(j) = j$. We regard them as the predicted values of the black hole mass and angular momentum. The difference of the total mass M and $m_{\rm f}$ can be regarded as the possible maximum mass of a disk surrounding the formed black hole. We note that infalling matter of a noncircular orbit with $j > j_{\rm ISCO}$ may fall into the black hole in reality, and thus, the black hole mass can be slightly larger than the predicted value (see right panel of Figure 5).

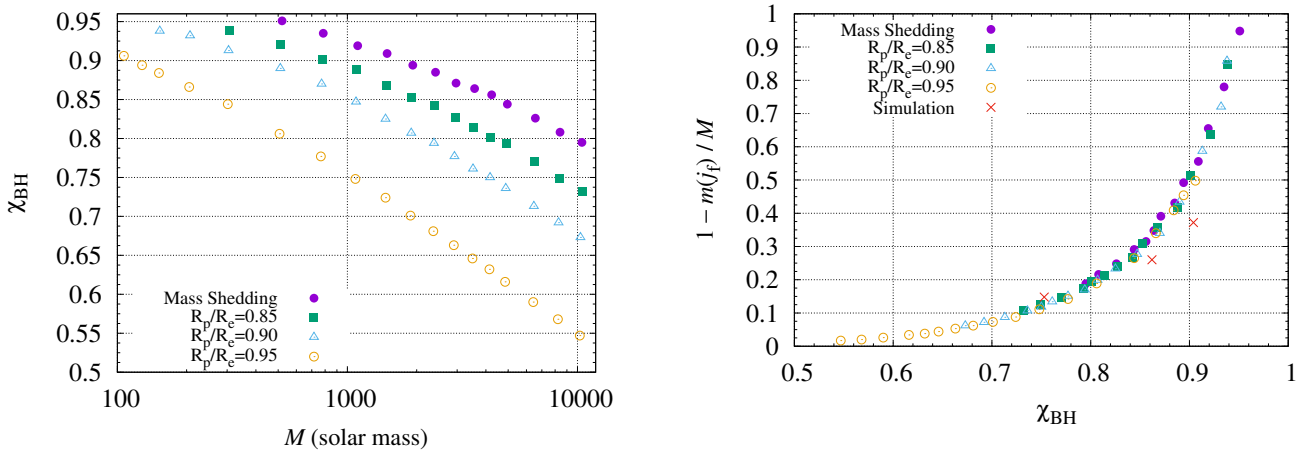

Figure 5. Left: predicted dimensionless spin of the hypothetically formed black hole, $\chi_{\rm BH}$, as a function of the core mass with fixed values of $R_{\rm p}/R_{\rm e} = 2/3$, 0.85, 0.90, and 0.95. Right: the same as the left panel, but for the predicted mass fraction of the matter located outside the black hole as a function of $\chi_{\rm BH}$. The cross marks denote the simulation results at 5 s after the black hole formation for $s = 35k$ and $R_{\rm p}/R_{\rm e} = 0.95$, 0.90, and 0.85 (from left to right).

Figure 5 shows the predicted black hole dimensionless spin defined by $\chi_{\rm BH} = cJ(j_{\rm f})/(Gm(j_{\rm f})^2)$ as a function of the initial mass M (left panel) and the maximum mass fraction that could be a disk defined by $1 - m(j_{\rm f})/M$ (right panel) as a function of $\chi_{\rm BH}$. For $R_{\rm p}/R_{\rm e} \lesssim 0.85$ and $M \lesssim 500\ M_\odot$, the plots are missing. The reason why we omit plotting is that, for such a parameter space, the dimensionless spin exceeds unity for a small black hole mass with $\lesssim 0.05M$. We speculate that for such cases, a black hole might not be formed but a rapidly rotating spheroid or torus is formed. We plot the results for a variety of s/k ($M \approx 10^2$–$10^4\ M_\odot$) with $R_{\rm p}/R_{\rm e} = 2/3$, 0.85, 0.90, and 0.95. For $R_{\rm p}/R_{\rm e} = 2/3$, the stellar core is approximately at the mass-shedding limit. We note that $M - m(j_{\rm f})$ denotes the maximum mass that could form a disk. As shown below, the disk mass fraction is smaller than this during the evolution of the system, because the matter is still falling toward the center in the early stages.

The left panel of Figure 5 shows that the black hole dimensionless spin is likely to be high $\gtrsim 0.8$ for $M \lesssim 10^3\ M_\odot$ even for moderately rapidly rotating cores with $R_{\rm p}/R_{\rm e} \lesssim 0.90$. In particular, for $M \lesssim 300\ M_\odot$, the dimensionless spin can be larger than 0.85 even for a stellar core with $R_{\rm p}/R_{\rm e} = 0.95$ for which $\Omega/\Omega_{\rm Kep}$ is $\approx$32%. Such cores can be a good progenitor model of the black holes of GW231123.

The right panel of Figure 5 shows that for $\chi_{\rm BH} \gtrsim 0.80$, 0.85, and 0.90, $\gtrsim$20%, 30%, and 50% of the initial mass, respectively, could form a disk irrespective of the angular velocity of the stellar core. This indicates that the formation of a rapidly spinning black hole would accompany the formation of a massive disk, which will be subsequently unstable to nonaxisymmetric deformation. It should be also noted that the black hole mass can be much smaller than the core mass for the rapidly rotating core collapse. For example, a black hole with mass $\sim 50\ M_\odot$ may be temporarily formed from a core with mass $\gtrsim 140\ M_\odot$ if the formed black hole is rapidly spinning (although after the evolution of the formed disk by nonaxisymmetric instability and/or viscous processes, the black hole mass would increase subsequently).

To confirm that our analysis is approximately valid, we perform axisymmetric simulations in general relativity. For this purpose, we pick up a stellar core with $s/k = 35$ and $R_{\rm p}/R_{\rm e} = 0.85$, 0.90, and 0.95. For these models, the core mass is ≈ 1.10, 1.09, and $1.08 \times 10^3\ M_\odot$, respectively. For the simulation, we use a code recently developed for a study of the collapse of supermassive stars (S. Fujibayashi et al. 2025), for which the Timmes–Swesty equation of state is employed. We include the neutrino emission cooling by pair processes, adopting the fitting formula in N. Itoh et al. (1996). We further implement a nuclear reaction network as in the manner of H. Uchida et al. (2019) and F. X. Timmes (1999) although for such massive stellar cores, the effect of the nuclear burning in the formation of a black hole and disk is minor. Simulations are performed on a nonuniform grid structure of cylindrical coordinates of ϖ-z with the three grid resolutions of $\Delta x/M = 0.015$, 0.010, and 0.007, where x denotes ϖ or z. The grid spacing is uniform for $x \lesssim GM/c^2$ and increased as $dx_{i+1} = 1.017dx_i$ for $x \gtrsim GM/c^2$, where x_i denotes the ith grid point.

Figure 6 shows the evolution of masses of the black hole, of the matter located outside the black hole, and of the disk approximately defined as a function of the time measured after the formation of the black hole in units of the initial mass (left) and the evolution of the dimensionless spin of the black hole for $R_{\rm p}/R_{\rm e} = 0.90$. Here, the mass and spin of the black hole are estimated by analyzing the area and circumferential radii of the apparent horizon (see, e.g., M. Shibata 2016). The disk is defined as a region in which the radial velocity is smaller than the rotational velocity. It is found that the black hole mass and dimensionless spin increase with time toward approximate constants. The relaxed values of the black hole mass and dimensionless spin decrease and increase, respectively, with the improvement of the grid resolution, and the convergence is not fully achieved in our choice of the grid resolution. However, it is reasonable to conclude that the masses of the black hole and the matter located outside the black hole at $t - t_{\rm BH} = 2$ s are $\approx 0.7M$ and $0.3M$ (i.e., $M_{\rm disk}/M_{\rm BH}$ can be $\sim$0.4), respectively, and the dimensionless spin is $\approx$0.86. These values agree approximately with those predicted from the initial configuration: in the right panel of Figure 5, the crosses denote the results with the finest grid resolution, and we find that the results indeed agree approximately with the prediction from the initial configuration.

Figure 7 shows the configuration of the rest-mass density (left) and entropy per baryon (right) of the disk at $t - t_{\rm BH} \approx 2$ s and 5 s. It is found that the density maximum is located at $\approx$3–4$GM_{\rm BH}/c^2$, and the high-density (and low-entropy) region is confined in the region of $\varpi \lesssim 15GM_{\rm BH}/c^2$ (note that $M_{\rm BH} \approx 8 \times 10^2\ M_\odot$, and thus, $GM_{\rm BH}/c^2 \approx 1.2 \times 10^8$ cm). This implies that a compact and massive disk is indeed formed immediately after the black hole

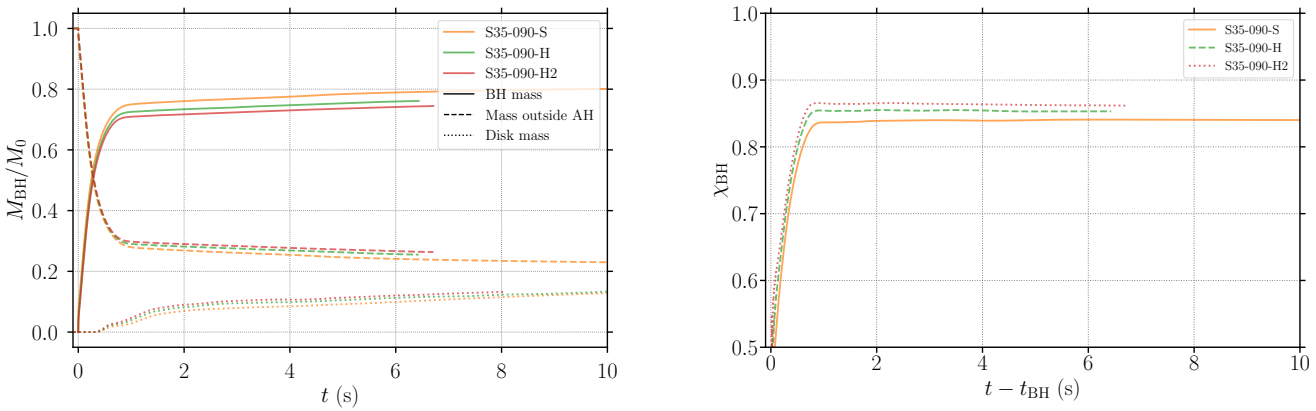

Figure 6. Left: evolution of masses of the black hole, of the matter located outside the black hole, and of the disk approximately defined as functions of time measured after the formation of the black hole, in units of the initial mass. Right: evolution of the dimensionless spin of the black hole. For both panels, the results for $R_{\rm p}/R_{\rm e} = 0.90$ are plotted. $t_{\rm BH}$ denotes the time at the formation of the black hole.

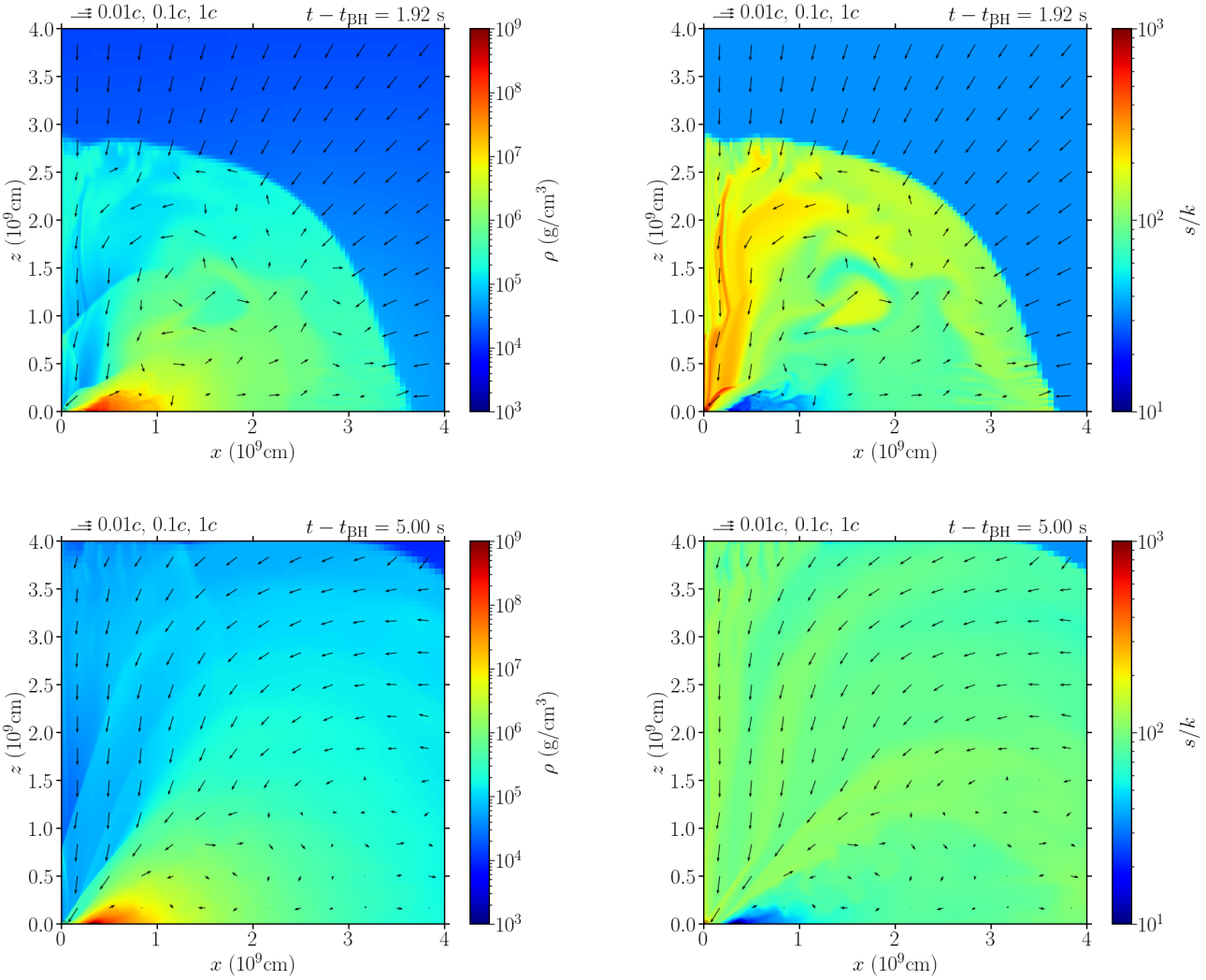

Figure 7. Configuration of the rest-mass density (left) and entropy per baryon (right) of the disk at $t - t_{\rm BH} \approx 2$ s (upper panel) and 5 s (lower panel) for the simulation of $s/k = 35$, $R_{\rm p}/R_{\rm e} = 0.90$, and $\Delta x = 0.007GM/c^2$.

formation, and in the subsequent time evolution, an extended region of the disk grows. In the high-density part of the disk, the values of s/k are approximately the same as the initial value, $s/k = 35$, except for a decrease due to neutrino cooling. This indicates that if the initial values of s/k are approximately preserved, a compact disk would be formed.

As Figure 6 shows, the mass of the disk increases with time gradually due to the matter infall from the outer region. As

previous studies showed (K. Kiuchi et al. 2011; M. Shibata et al. 2021), the more massive (and more compact) disk can be more unstable to nonaxisymmetric deformation. Hence, it is not clear at what time the most intense instability sets in during the evolution of the disk. To fully understand the mechanism of the nonaxisymmetric instability, we need a three-dimensional simulation, which we plan to perform in future work. However, the present result clearly shows that a massive disk is formed, and therefore, gravitational waves associated with the nonaxisymmetric deformation of the massive disk should be emitted after the collapse of rotating very massive stellar cores to a black hole.

We performed similar simulations for $R_p/R_e = 0.85$ and 0.95. For these models, the masses of the black hole and matter located outside the black hole and the dimensionless spin of the black hole approach $\approx 0.6M$, $0.4M$, and 0.91 for $R_p/R_e = 0.85$ and $\approx 0.9M$, $0.1M$, and 0.75 for $R_p/R_e = 0.95$, respectively. The dimensionless spins of the black holes are broadly consistent with those predicted from the initial data (see cross marks in the right panel of Figure 5). The value of $M - m(j_f)$ for the rapidly spinning case with $R_p/R_e = 0.85$ is slightly smaller than the prediction from the initial data, but it is clearly shown that the high initial rotation can enhance the fraction of the matter located outside the black hole.

5. Discussion

In this section, we predict the frequency and amplitude of gravitational waves emitted by unstable disks, assuming that disks are formed around a black hole after the stellar collapse of very massive stars. For this purpose, we extrapolate the results in our previous paper (M. Shibata et al. 2021).

M. Shibata et al. (2021) performed fully general relativistic simulations for massive disks with mass of $M_{\rm disk} = 15$–$50\ M_\odot$ orbiting a spinning black hole with mass of $M_{\rm BH} \approx 50\ M_\odot$ and dimensionless spin of $\chi_{\rm BH} \approx 0.8$. They considered disks with the maximum density located at $R_{\rm peak} = 7$–$9\ r_g$, where $r_g = GM_{\rm BH}/c^2$. They found that for all cases, the disk is nonaxisymmetrically unstable to the formation of a spiral arm and becomes a burst source of gravitational waves. They also showed that some of the waveforms are similar to the observed waveform of GW190521 (R. Abbott et al. 2020; and also to that of GW231123, A. G. Abac et al. 2025): the waveforms are composed primarily of a few burst waves with high amplitude and subsequent quasiperiodic waves with relatively low amplitude.

The typical frequency of gravitational waves (in the source frame) found in M. Shibata et al. (2021) is written approximately as

$$f_{\rm GW} \approx 0.8 \frac{c}{\pi r_g} \left(\frac{R_{\rm peak}}{r_g} \right)^{-3/2}, \tag{3}$$

and for $M_{\rm BH} = 50\ M_\odot$, it is 40–60 Hz. Here, the approximate factor of 0.8 comes from the fact that the spiral arm is formed in an extended region of $r > R_{\rm peak}$. The maximum amplitude of gravitational waves emitted is written as

$$h_{\rm eff} = \epsilon \frac{GM_{\rm disk} r_g}{c^2 D R_{\rm peak}} \approx 3 \times 10^{-22} \left(\frac{\epsilon}{0.2} \right) \left(\frac{M_{\rm disk}}{20 M_\odot} \right) \times \left(\frac{R_{\rm peak}}{7 r_g} \right)^{-1} \left(\frac{D}{100\ {\rm Mpc}} \right)^{-1}, \tag{4}$$

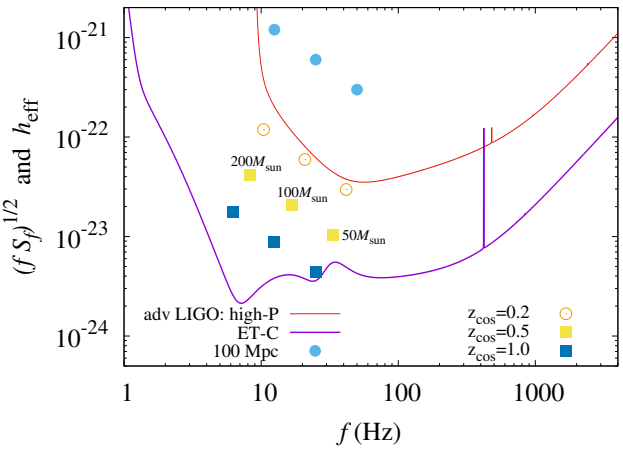

Figure 8. Comparison of the predicted effective amplitude of gravitational waves for $M_{\rm BH} = 200$, 100, and $50M_\odot$ and designed sensitivity curves of the advanced LIGO and Einstein Telescope of the configuration-type C (the dimensionless quantity, $(f\ S_f)^{1/2}$, is defined from the sensitivity curve S_f). We choose $\epsilon = 0.2$, $M_{\rm disk}/M_{\rm BH} = 0.4$, and $R_{\rm peak}/r_g = 7$ for the plot of the effective amplitude. The luminosity distances are chosen to be 100 Mpc, and the luminosity distances of the cosmological redshift $z_{\rm cos} = 0.2$, 0.5, and 1.0. The cosmological effects are taken into account to plot the effective amplitude and frequency.

where D denotes the luminosity distance to the source, ϵ is approximately in the range between 0.1 and 0.3, and the gravitational-wave amplitude is consistent with the prediction by the quadrupole formula. We note that the value of ϵ depends on the compactness (or equivalently, the entropy per baryon) of the disk.

We here focus on the cases that the disk mass is 30%–60% of the black hole mass and extrapolate our previous results for higher black hole masses with $M_{\rm BH} \gtrsim 100\ M_\odot$. For this case, the gravitational-wave frequency becomes lower, as

$$f_{\rm GW} \approx 28\ {\rm Hz} \left(\frac{M_{\rm BH}}{100 M_\odot} \right)^{-1} \left(\frac{R_{\rm peak}}{7 r_g} \right)^{-3/2}. \tag{5}$$

On the other hand, the disk mass is larger for a fixed ratio of $M_{\rm disk}/M_{\rm BH}$.

Figure 8 plots the predicted effective amplitudes and frequencies of gravitational waves for $\epsilon = 0.2$, $M_{\rm disk}/M_{\rm BH} = 0.4$, and $R_{\rm peak}/r_g = 7$ and compares them with the designed sensitivity curves of the advanced LIGO and Einstein Telescope of the configuration-type C (S. Hild et al. 2011).[6] This shows that, with the current detectors, the events for $M_{\rm BH} = 100$–$200\ M_\odot$ can be detected only when the distance to the source is less than $\sim$100–200 Mpc. On the other hand, by the Einstein Telescope, for which the sensitivity in the lower-frequency band $\lesssim$30 Hz is much better than that of the advanced LIGO, the events with $M_{\rm BH} = 100$–$200\ M_\odot$ may be detected up to $z_{\rm cos} \sim 1$. As the supernova rate increases with the increase of $z_{\rm cos}$ (see, e.g., T. Pessi et al. 2025), and the metallicity of massive stars should be lower for higher cosmological redshifts, it may be expected that the formation rate of the very massive stars leading to black hole formation can be higher than that in the current Universe. This suggests that the collapse of rotating very massive stellar cores at $z_{\rm cos} \lesssim 1$ can be a source of the Einstein Telescope for a lower-frequency band of $f_{\rm GW} \sim 10$–20 Hz; if the formation of massive black holes similar to the black holes of GW231123 is frequently

[6] See also https://www.et-gw.eu/index.php/etsensitivities.

formed for $z_{\rm cos} \lesssim 1$, the formation process itself is a promising source for the Einstein Telescope.

Our numerical simulations for $s/k = 35$ show that $R_{\rm peak}/r_g$ is appreciably smaller than 7. If this is also the case for smaller values of s/k, by which black holes of $M_{\rm BH} = 50$–$200\ M_\odot$ are formed, the frequency and amplitude of gravitational waves considered here are higher and larger, respectively. We plan to systematically investigate this point in our future numerical work.

One concern associated with the detection of this type of burst gravitational wave is that the waveforms can be mistaken for that of a binary black hole merger because two gravitational waveforms are similar for the highest-amplitude part. An advantage for the gravitational collapse case is that this type of event is likely to be accompanied by electromagnetic emissions, which can be driven by a disk wind (H. Uchida et al. 2019; D. M. Siegel et al. 2022; A. Agarwal et al. 2025) and/or a jet (O. Gottlieb et al. 2025). Thus, the detection of some electromagnetic counterparts will be the key to confirming that the gravitational-wave event is associated with the gravitational collapse of a very massive star.

6. Summary

We derived and analyzed equilibrium states of rotating oxygen cores that are marginally stable against pair instability. We showed that for relatively low-mass cores with $M \lesssim 10^3\ M_\odot$, the radius of the cores in units of the gravitational radius can be quite large, $\gtrsim$1500, and thus, even in the presence of a moderately rapid rotation, the rotational effect at the formation of a black hole can be significant. Specifically, if the core rotates with $\Omega/\Omega_{\rm Kep} \gtrsim 0.3$, the mass of the disk can be $\gtrsim$30% of the initial core mass; a black hole can be surrounded by a massive disk that is subsequently unstable to nonaxisymmetric instability and can be a strong emitter of gravitational waves.

Using results in our previous study on the evolution of unstable massive disks orbiting a black hole (M. Shibata et al. 2021), we estimated the effective amplitude and frequency of gravitational waves emitted from the massive disk, assuming that the disk mass is 30%–60% of the black hole mass. We indicated that the black hole–disk systems with $M_{\rm BH} \approx 100$–$200\ M_\odot$ formed for $z_{\rm cos} \lesssim 1$ can be a source of the Einstein Telescope for the frequency band of $\sim$10–20 Hz.

In the present paper, we extrapolated the previous results of M. Shibata et al. (2021) to infer the properties of gravitational waves, assuming that the scaling relation for the amplitude and frequency with respect to the black hole mass is satisfied. Although this assumption is likely to be valid, it is desirable to perform a numerical simulation with a more strict setup for the masses of the black hole and disk. More desirable is to perform a simulation from the stellar core collapse throughout the formation of a black hole–disk system, which is subsequently unstable for the emission of gravitational waves. We plan to perform such a self-consistent simulation in subsequent work (A T.-L. Lam et al. 2025, in preparation). Exploring the long-term evolution of the disk is also an important subject to determine the final mass and spin of the black hole.

In M. Shibata et al. (2021), we pointed out that the waveforms of another massive binary black hole merger, GW190521 (R. Abbott et al. 2020), could be mimicked by gravitational waves from black hole–massive disk systems for which the disk is deformed nonaxisymmetrically. This could also be the case for GW231123; similar waveforms may be derived by a model of black hole–disk systems. It is interesting to pursue this possibility as well.

Acknowledgments

We thank Koh Takahashi for the useful discussion and for sharing the data of stellar evolution models. We also thank Kenta Hotokezaka for the helpful conversation. Numerical computation was performed on the cluster Sakura and Momiji at the Max Planck Computing and Data Facility. This work was in part supported by Grant-in-Aid for Scientific Research (grant No. 23H04900) of Japanese MEXT/JSPS.

ORCID iDs

Masaru Shibata https://orcid.org/0000-0002-4979-5671
Sho Fujibayashi https://orcid.org/0000-0001-6467-4969

References

Abac, A. G., Abouelfettouh, I., Acernese, F., et al. 2025, ApJL, 993, L25
Abbott, R., Abbott, T. D., Abraham, S., et al. 2020, PhRvL, 125, 101102
Agarwal, A., Siegel, D. M., Metzger, B. D., & Nagele, C. 2025, arXiv:2503.15729
Arnett, D. 1996, Supernovae and Nucleosynthesis: An Investigation of the History of Matter from the Big Bang to the Present (Princeton Univ. Press)
Bardeen, J. M., Press, W. H., & Teukolsky, S. A. 1972, ApJ, 178, 347
Bond, J. R., Arnett, W. D., & Carr, B. J. 1984, ApJ, 280, 825
Chandrasekhar, S. 1964, ApJ, 140, 417
Croon, D., Sakstein, J., & Gerosa, D. 2025, arXiv:2508.10088
Fryer, C. L., Woosley, S. E., & Heger, A. 2001, ApJ, 550, 372
Fujibayashi, S., Jockel, C., Kawaguchi, K., Sekiguchi, Y., & Shibata, M. 2025, ApJ, 981, 119
Fujibayashi, S., Lam, A. T.-L., Shibata, M., & Sekiguchi, Y. 2024, PhRvD, 109, 023031
Gottlieb, O., Metzger, B. D., Issa, D., et al. 2025, ApJL, 993, L54
Heger, A., & Woosley, S. E. 2002, ApJ, 567, 532
Hild, S., Abernathy, M., Acernese, F., et al. 2011, CQGra, 28, 094013
Itoh, N., Hayashi, H., Nishikawa, A., & Kohyama, Y. 1996, ApJS, 102, 411
Kıroğlu, F., Kremer, K., & Rasio, F. A. 2025, ApJL, 994, L37
Kiuchi, K., Shibata, M., Montero, P. J., & Font, J. A. 2011, PhRvL, 106, 251102
Korobkin, O., Abdikamalov, E. B., Schnetter, E., Stergioulas, N., & Zink, B. 2011, PhRvD, 83, 043007
Pessi, T., Desai, D. D., Prieto, J. L., et al. 2025, A&A, 703, A34
Popa, S. A., & de Mink, S. E. 2025, arXiv:2509.00154
Shapiro, S. L., & Teukolsky, S. A. 1983, Black Holes, White Dwarfs and Neutron Stars. The Physics of Compact Objects (Wiley)
Shibata, M. 2004, ApJ, 605, 350
Shibata, M. 2016, Numerical Relativity (World Scientific)
Shibata, M., Fujibayashi, S., Jockel, C., & Kawaguchi, K. 2025, ApJ, 978, 58
Shibata, M., Fujibayashi, S., Lam, A. T.-L., Ioka, K., & Sekiguchi, Y. 2024, PhRvD, 109, 043051
Shibata, M., Kiuchi, K., Fujibayashi, S., & Sekiguchi, Y. 2021, PhRvD, 103, 063037
Shibata, M., & Shapiro, S. L. 2002, ApJL, 572, L39
Shibata, M., Uchida, H., & Sekiguchi, Y. 2016, ApJ, 818, 157
Siegel, D. M., Agarwal, A., Barnes, J., et al. 2022, ApJ, 941, 100
Stegmann, J., Olejak, A., & de Mink, S. E. 2025, ApJL, 992, L26
Takahashi, K., Yoshida, T., & Umeda, H. 2018, ApJ, 857, 111
Takahashi, K., Yoshida, T., Umeda, H., Sumiyoshi, K., & Yamada, S. 2016, MNRAS, 456, 1320
Tanikawa, A., Liu, S., Wu, W., Fujii, M. S., & Wang, L. 2025, arXiv:2508.01135
Tassoul, J.-L. 1978, Theory of Rotating Stars (Princeton Univ. Press)
Timmes, F. X. 1999, ApJS, 124, 241
Timmes, F. X., & Swesty, F. D. 2000, ApJS, 126, 501
Uchida, H., Shibata, M., Takahashi, K., & Yoshida, T. 2019, ApJ, 870, 98
Zeldovich, Y. B., & Novikov, I. D. 1971, Relativistic Astrophysics. Vol. 1: Stars and Relativity (Univ. of Chicago Press)